PALEOSECULAR VARIATION AND ABSOLUTE GEOMAGNETIC PALEOINTENSITY RECORDS RETRIEVED FROM THE EARLY CRETACEOUS POSADAS FORMATION (MISIONES, ARGENTINA)

MABEL MENA[1], AVTO GOGUITCHAICHVILI[2], MIGUEL CERVANTES SOLANO[2] AND JUAN FRANCISCO VILAS[1]

1 Instituto de Geofísica Daniel Valencio, Dpto. Ciencias Geológicas, Facultad de Ciencias Exactas y Naturales, Universidad de Buenos Aires, Argentina (mena@gl.fcen.uba.ar)

2 Laboratorio Interinstitucional de Magnetismo Natural, Instituto de Geofísica - Sede Michoacán, Universidad Nacional Autónoma de México, Campus Morelia, 58089 Morelia, Mexico (avto@geofisica.unam.mx)

Received: February 26, 2010; Revised: July 6, 2010; Accepted: October 17, 2010

ABSTRACT

The Early Cretaceous may be considered a key period for understanding the evolution of the Earth's magnetic field. Some still unsolved problems are related to the mode of paleosecular variation (PSV) of the Earth's magnetic field before and during the Cretaceous Normal Superchron. We report here a detailed rock-magnetic, paleomagnetic and paleointensity investigation from 28 lava flows (331 standard paleomagnetic cores) collected in the Argentinean part of the Parana Flood Basalts (Formation Posadas) in order to contribute to the study of PSV during the early Cretaceous and to obtain precise Cretaceous paleomagnetic pole positions for stable South America. The average paleofield direction is precisely determined from 26 sites, which show small within-site dispersion and high directional stability. Five sites show evidences for the self-reversal of thermoremanent magnetization. 23 sites yielded normal polarity magnetization and only 3 are reversely magnetized. Moving windows averages were used to analyze the sequential variation of virtual geomagnetic pole's (VGP) axial positions. Interestingly, the axial average VGP path traces an almost complete cycle around the geographical pole and passes near the location of all previously published Paraná Magmatic Province poles. Both paleomagnetic poles and average VGP paths are significantly different from the pole position suggested by fixed hotspot reconstructions, which may be due to true polar wander or the hotspot motion itself. Only 15 samples from 5 individual basaltic lava flows, yielded acceptable paleointensity estimates. The site mean paleointensities range from 25.2 ± 2.2 to 44.0 ± 2.2 μT. The virtual dipole moments (VDMs) range from 4.8 to 9.9 × 10^{22} Am^2. This correspond to a mean value of 7.7 ± 2.1 × 10^{22} Am^2 which is 96% of the present day geomagnetic field strength. These intensities agree with the relatively high values already reported for Early Cretaceous, which are consistent with some inferences from computer simulations previously published.

Continuation of LATINMAG Special Issue #4, Stud. Geophys. Geod., **54** (2010)

Keywords: paleosecular variation, Early Cretaceous, paleomagnetic poles, Paraná Magmatic Province, Argentina, Posadas Formation.

1. INTRODUCTION

The study of fluctuations of the Earth's magnetic field in the geological past, in terms of both absolute intensity and directions, are of great interest in geophysics. Therefore, knowledge of geomagnetic variations with geological time is essential for understanding the functioning of the geodynamo, which is intimately connected to conditions in the Earth's liquid core and at the core-mantle boundary (*Hide, 1967*; *Courtillot and Besse, 1987*; *Gubbins, 1994*; *Glatzmaier and Roberts, 1995*; *Heller at al., 2002*). These data provide thus an important source of information on the physics of the Earth's deep Interior.

Considering the polarity time scale for the last 160 Ma, it is seen that the length of the majority of polarity intervals lies in the time range of 0.1 to 1 Ma. The Cretaceous Normal Superchron (CNS) is a clear outlier with duration of about 35 Ma from 118 to 83 Ma (*Cande and Kent, 1995*; *Tarduno et al., 2002*). Thus this period cannot be accommodated in the rest of the polarity sequence, therefore suggesting that the geodynamo must have two fundamental states: a reversing and a non-reversing states (*McFadden and Merrill, 1997*). *Larson and Olson (1991)* found that the magnetic field will cease to change polarity if the amplitude of convection in the outer core rises above some threshold, and they speculated that the CNS (i.e. non-reversing state of the geodynamo) corresponds to a period with strong convection in the Earth's outer core. They also predicted an abnormally high paleointensity of the geomagnetic field during the CNS. Hence, new high quality paleomagnetic data from the Early Cretaceous are important in order to both constrain geodynamo theory and provide a mean for better understanding the long term evolution of the geodynamo.

For these reasons, we investigated 28 independent lava flows (331 standard paleomagnetic cores) erupted during the Early Cretaceous in northeastern Argentina, which have several advantages: (1) they are widely distributed in a large volcanic province and easy to access; (2) they record faithfully the magnetic field that existed at the time of their eruption (*Mena et al., 2006*); (3) the age of these eruptions are well constrained.

2. GEOLOGICAL SETTING AND SAMPLING DETAILS

The basalts of the Posadas Formation (*Gentili and Rimoldi, 1980*), which outcrop in north-eastern Argentina, belong to the Paraná Magmatic Province (PMP), considered as one of the largest continental volcanic provinces in the world (*Ernesto et al., 1990*). These lava flows were extruded during the huge continental volcanism that affected the Paraná Basin in the Lower Cretaceous. The volcanic outcrops extend into Paraguay, Uruguay and South Brazil where they are called Alto Paraná, Arapey and Serra Geral Formation, respectively. Coetaneous volcanic rocks are also exposed in Africa, forming the Etendeka-Angola igneous province (*Renne et al., 1992; 1996*). Available radiometric ages indicate the relatively short time interval from 137 to 127 Ma as the best estimate of the lava emplacements (*Turner et al., 1994*).

The PMP is divided into three parts, northern, central and southern, by the Rio Piquiri and Rio Uruguay tectonic lineaments (Fig. 1). This division is in accordance with petrological and geochemical features (*Piccirillo and Melfi, 1988*). Geochemically, the dominant rock type is tholeiitic basalt characterized by decrease of the TiO_2 content from the north to the south. The present study was carried out on lava flow outcrops in the central part of the PMP, in Misiones Province, Argentina. These rocks were classified as tholeiitic basalts and andesi-basalts characterized by a low to intermediate content of Ti (*Mena et al., 2006*).

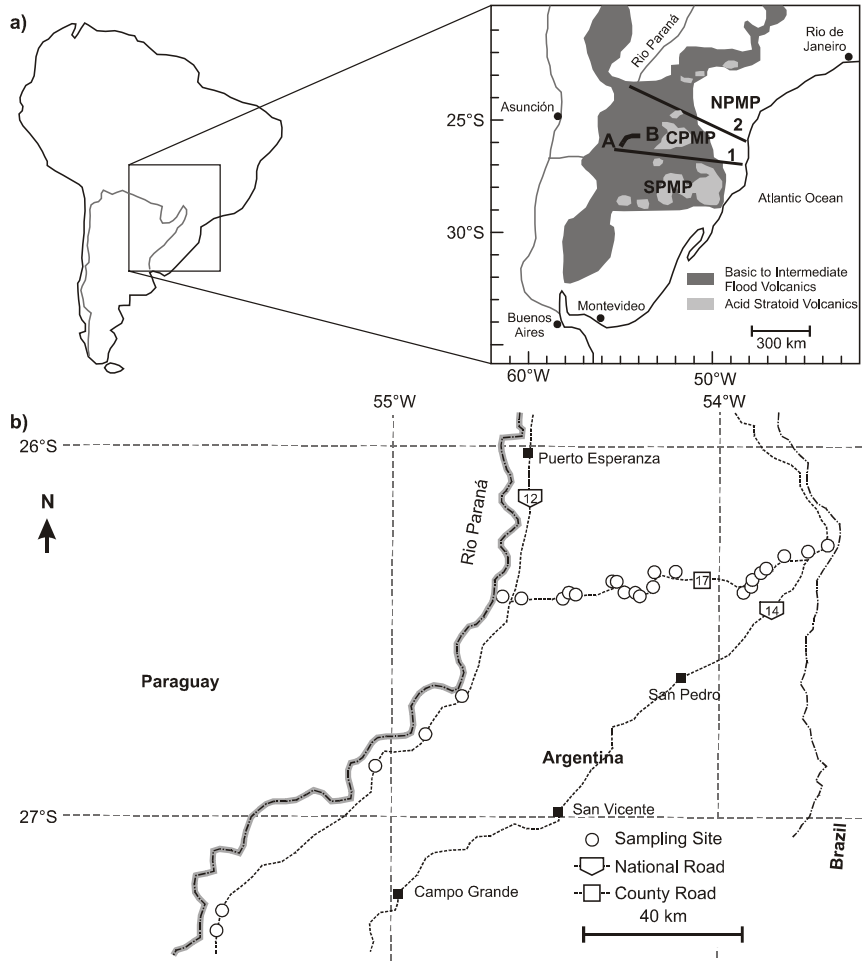

Fig. 1. **a)** Sketch map of Paraná Flood basalts. Thick black lines indicate Río Uruguay (1) and Río Piquiri (2) tectonic lineaments which divide the Paraná Magmatic Province into three mayor parts: northern (NPMP), central (CPMP) and southern (SPMP) (after *Piccirillo and Melfi, 1988*); thick A-B line indicates the sampling sections. **b)** Sketch map of the Misiones province, Argentina and locations of the sampling sites.

Paleomagnetic samples were extracted along the roads between San Ignacio, Eldorado and Bernardo de Irigoyen localities (Fig. 1). The lava flows are well exposed in the road cuts with sub-horizontal position. Five sites were located between San Ignacio and Eldorado. The first of them corresponds to a basaltic flow situated about 40 m above the contact with underlying Solari Formation - equivalent to the Botucatú Formation in Brazil. Due to the relatively high alteration, the rocks near the contact are inadequate for paleomagnetic studies. The remaining 23 sites were located between Eldorado and Bernardo de Irigoyen towns.

Ernesto et al. (1990) reported first comprehensive paleomagnetic study from more than 300 sites belonging to PMP. This pioneering study however presents a major limitation because only three oriented hand samples per site are investigated and thus does not meet the basic criteria to study the fine characteristics of geomagnetic paleosecular variation (*Biggin et al., 2008*). The same is true for the study conducted by *Mena et al. (2006)* who only used one or two hand samples on the Argentinean part of PMP (Posadas Formation). This later study should be considered as reconnaissance and thus cannot be used as supplementary material for present modern paleomagnetic survey. Based on field observations and absolute altitudes, it was possible to establish a relative stratigraphy of the studied lava flows. Because these lava flows were extruded in a complex paleorelief in context of some vertical displacements along sub-vertical faults, their sequential positions are not necessarily indicative of their relative ages. A total of 331 standard paleomagnetic cores were drilled at the 28 sites and oriented with both magnetic and sun compasses whenever possible.

The stratigraphic position of sites, determined in function of geological/field observation and absolute altitudes allowed to establish a relative sequence, from bottom to top: 1SG through 11SG, 13SG, 12SG 15SG, 14SG and 16SG through 28SG. Microscopic observations carried out on polished and thin sections under reflected and transmitted light show a porphyritic texture, with olivine phenocrysts, frequently altered to iddingsite (an alteration of olivine that consists of a mixture of clay minerals, iron oxides and ferrihydrites). On the basis of their optical characteristics, opaque minerals seems to be mainly titanomagnetites and, to a much lesser extent, ilmenite. In some sections titanomaghemite appears in relatively small proportions acting as a replacement of titanomagnetite.

3. ROCK MAGNETISM

In order to identify the carriers of the remanent magnetization, to obtain information about their paleomagnetic stability and to assess the suitability of the collected samples for paleointensity studies, several rock-magnetic experiments were carried out. These experiments included: a) measurements of the viscosity index, b) measurements of continuous thermomagnetic curves (susceptibility versus temperature), and c) hysteresis experiments.

To obtain precise and reliable remanent magnetization (RM) measurements during the progressive thermal demagnetization it is advisable that the specimen has low magnetic viscosity. *Xu et al. (1986)* suggested that viscous remanences can be acquired very quickly but in spite of this they can decay much more slowly, and that this process can

operate in a wide variety of types of rocks. This phenomenon, probably due to an effect of later diffusion (*Néel, 1955*), could also reduce the accuracy of the RM measurements when the rocks are not treated and measured in a non magnetic atmosphere. In this study the index of viscosity *v* (*Thellier and Thellier, 1944*) was determined using two specimens per flow. Their RMs were measured at two moments: the first one after two weeks of storage with the cylindrical axis of the specimens parallel to environmental field and the other after having elapsed other two weeks of storage with axes in the opposite direction. The studied samples show low capacity to acquire viscous remanent magnetizations. The index of viscosity varies between 0.3 and 11.4% most being smaller than 5%.

Magnetic bulk susceptibility measurements κ at room temperature using dual frequencies of 470 and 4700 Hz (κ_{470} and κ_{4700}, respectively) were carried out for all specimens using a Bartington MS2 susceptibility meter. Some specimens of the 6SG, 21SG, 22SG and 26SG sites have *F* factors ($F = 100\left(\kappa_{470} - \kappa_{4700}\right)/\kappa_{470}$) between 7 and 11% suggesting the presence of superparamagnetic particles (SP) (*Dunlop and Özdemir, 1997*; *Evans and Heller, 2003*).

Low-field susceptibility measurements (κ-*T* curves) under air were carried out using a Highmoore susceptibility bridge equipped with furnace. Selected samples were heated up to about 600°C at a heating rate of 20°C/min and then cooled at the same rate. Curie temperature was determined by the method of *Prévot et al. (1983*).

In most cases, two different thermomagnetic phases were recognized during heating (Fig. 2, samples 13SG, 4SG, 6SG and 7SG). The lower Curie point ranges between 380–420°C, and the highest one is about 580°C. The cooling curve shows only a single phase, with a Curie temperature close to that of magnetite. Such irreversible curves can be explained by titanomaghemite, which probably transformed into magnetite (*Readman and O'Reilly, 1972*; *Özdemir, 1987*) during heating. Both experimental and theoretical studies (*Heider and Dunlop, 1987*; *Özdemir and Dunlop, 1989*; *Nishitani and Kono, 1989*; *Goguitchaichvili et al., 2000*) show that chemical remagnetization by maghemitization records the same field direction as the original thermoremanent magnetization (*TRM*). Consequently, paleodirections were most probably unaffected by alteration. Other samples, however, yielded reasonably reversible curves (Fig. 2, samples 16SG and 26SG) pointing to Ti-poor titanomagnetites as main magnetic carrier. It is worth to note that some (titano)hematite may be present in the studied samples but because of their low susceptibility signal it cannot be detected.

Hysteresis measurements at room temperature were performed on all studied samples using the AGFM 'Micromag' apparatus in fields up to 1.2 T. The saturation remanent magnetization (J_{rs}), the saturation magnetization (J_s) and coercitive force (H_c) were calculated after correction for the paramagnetic contribution. The coercivity of remanence (H_{cr}) was determined by applying progressively increasing backfield after saturation. The typical hysteresis loop is presented in Fig. 3. In general, the curves are symmetrical with no evidence of potbellied or wasp-waisted forms (*Tauxe et al., 1996*) detected, which probably reflects very restricted ranges of the opaque mineral coercivities. 'Small' pseudo-single-domain grains seem to be responsible for remanence judging from hysteresis parameters values (*Day et al., 1977*; *Dunlop and Özdemir, 1997*). Alternatively this behavior may be due to the presence of mixture of multi-domain (MD) and significant

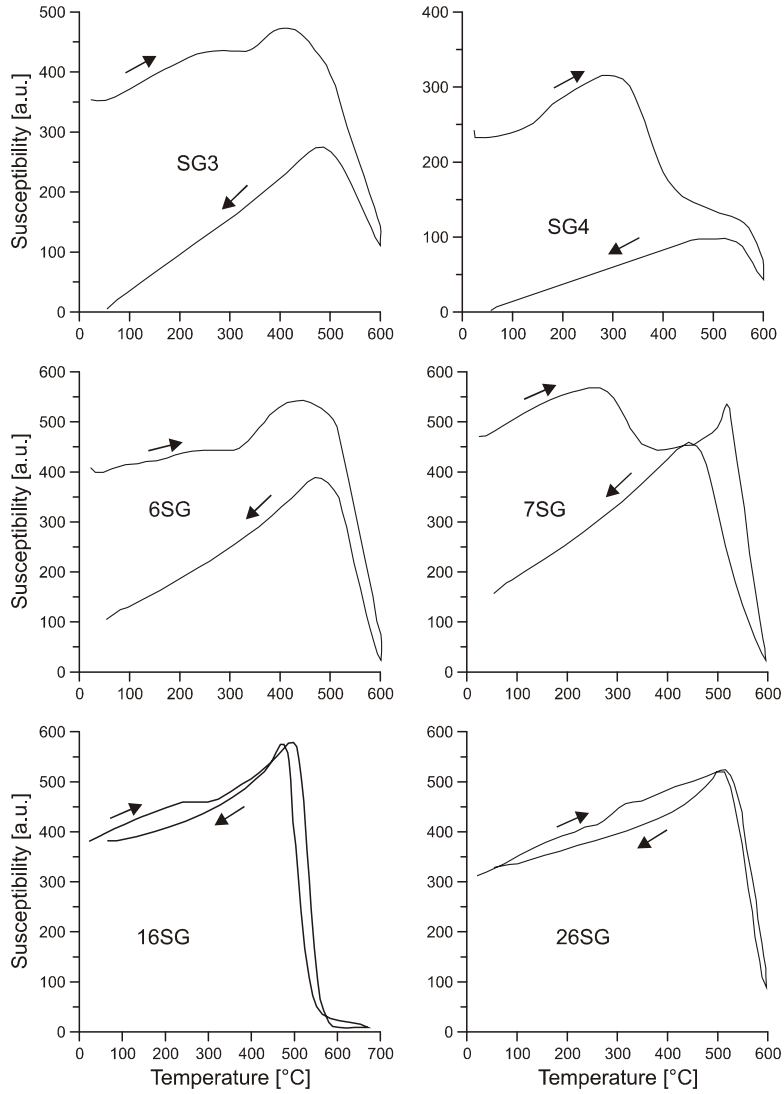

Fig. 2. Susceptibility versus temperature (in air) curves of representative samples. The arrows indicate the heating and cooling curves.

amount of single-domain (SD) grains. Let us note, that the domain state estimation using room temperature hysteresis parameters in terms of the plot of magnetization ratio versus coercivity ratio has no great resolution for most of natural rocks.

Based on the experimental study of the chemically well-identified synthetic titanomagnetites, *Day et al. (1977)* proposed an empiric relation between the domain

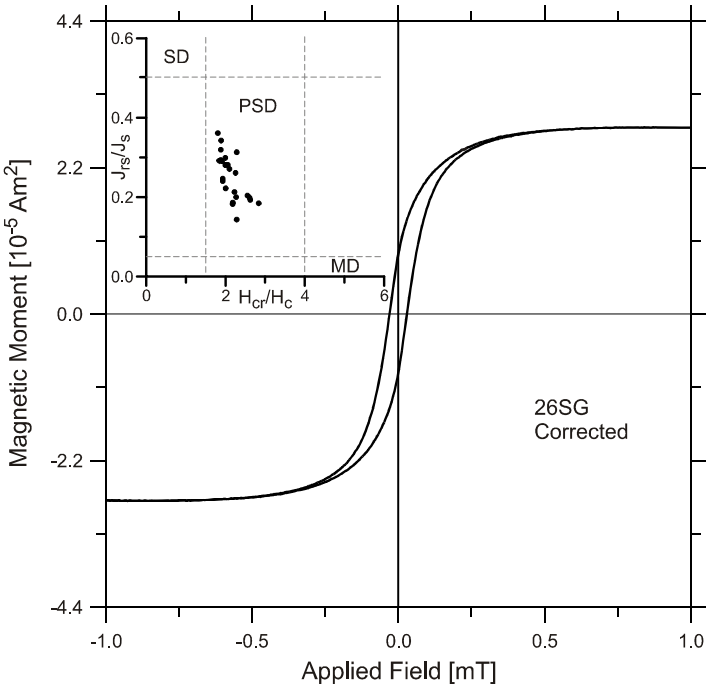

Fig. 3. Typical example of hysteresis loops (corrected for dia/paramagnetism) of small chip samples from the studied volcanic units and Day plot (*Day et al., 1977*) showing the relationship among different hysteresis parameters.

structure and the hysteresis parameters. However, natural rocks, almost always plot on the pseudo-single-domain behavior judging from their hysteresis parameter values. This is true for Posadas basalts too. As suggested by *Goguitchaishvili et al. (2001)*, natural rocks are complex magnetic systems, which contain the grains of variable sizes, coercivities and even distinct magnetic phases. Thus, generalizations based on studies of synthetic materials with perfectly established chemical composition is probably delicate. Let us note that if some superparamagnetic fraction exists also in these samples, the measured coercive force and saturation magnetization are somewhat lower and larger, (see for instance in *Dunlop, 2002*), respectively, than those ferrimagnetic fractions alone. Isothermal remanent magnetization (IRM) acquisition curves (not shown) were very similar for all samples. Saturation is reached in moderate fields of the order of 100–200 mT, which reveals that a cubic phase is the principal remanence carrier.

4. ANALYSIS OF THE PALEOMAGNETIC DIRECTIONS

Magnetic remanences were analyzed for one specimen from each core, employing both stepwise alternating magnetic field (AF) and thermal demagnetization techniques. Two specimens per site were submitted to thermal demagnetization and at least five

Table 1. Paleomagnetic results of studied section. *D*, *I* - declination and inclination of the site mean directions; *N* is number of specimens used; *k* and α_{95} are Fisherian statistical parameters; VGP Long, VGP Lat - longitude and latitude of the virtual geomagnetic poles.

Site	Polarity	*D*	*I*	*N*	*k*	α_{95}	VGP Long [°E]	VGP Lat [°S]
1	N	1.0	–55.4	9	55.84	6.9	299.1	–81.3
2	N	4.3	–53.3	10	454.21	2.3	276.2	–82.4
3	N	23.3	–35.0	8	87.67	5.9	200.4	–67.3
4	N	349.5	–48.0	7	97.54	6.1	19.1	–80.5
5	N	27.7	–50.7	8	91.36	5.8	232.9	–65.4
6	N	358.4	–51.3	7	359.02	3.2	319	–84.3
7	N	333.4	–47.8	6	352.07	3.6	23.2	–66.4
8	N	10.2	–38.2	9	52.48	7.2	189.8	–79.5
9	N	13.5	–51.0	8	169.93	4.3	242.9	–77.1
10	N	11.5	–48.4	5	301.90	4.4	234.6	–79.4
11	N	1.0	–41.0	8	257.91	3.5	143.2	–87.0
13	N	354.9	–31.7	6	322.10	3.7	97.6	–79.6
12	N	359.9	–31.9	10	113.00	4.6	125.2	–80.9
15	N	356.8	–29.0	5	83.20	3.0	109.8	–78.7
14	N	358.8	–35.0	9	376.49	2.7	116.7	–82.8
16	N	352.5	–33.6	8	249.47	3.5	83.4	–79.4
17	N	359.8	–39.8	5	404.39	3.8	123	–86.2
18	R	172.8	66.1	6	87.04	7.2	318.2	–67.2
19	R	167.9	42.1	2	267.11	15.3	43.7	–78.9
20	N	354.8	–44.9	6	53.18	9.3	32.9	–85.3
21	R	171.1	54.2	8	46.33	8.2	346.5	–78.7
22	R	177.5	47.3	8	224.11	3.7	340.3	–86.7
23	N	356.8	–46.6	5	257.65	4.8	7.2	–86.8
24	N	358.7	–42.4	7	265.98	3.7	92.6	–87.9
25	N	351.6	–37.6	6	119.37	6.2	68.8	–80.7
26	N	3.6	–52.3	8	29.27	10.4	281.7	–82.7
27	N	357.6	–40.2	8	50.67	7.9	92.8	–86.0
28	N	356.5	–42.7	11	55.63	6.2	60.9	–86.5
Secondary Components								
19	N	356.2	–39.2	7	235.38	3.9	85.3	–84.6
21	N	32.8	–51.4	4	16.73	23.1	235.3	–60.9
22	N	357.4	–50.1	8	32.39	9.9	352.1	–86.9
23	R	182.4	47.7	2	171.74	21.0	265.7	–86.8
27	R	176.0	29.1	4	24.37	18.0	106.2	–78.6
28	R	165.2	36.6	8	160.05	4.4	56.7	–75.2

specimens per site were treated by AF demagnetization. Remanent magnetization measurements and demagnetizations were performed with a DC-squids 2G cryogenic magnetometer with an incorporated three-axis static AF demagnetizer and an ASC-Scientific thermal demagnetizer.

Thermal demagnetization (TD) was performed in 12 steps from 100°C to 600°C. In few cases two additional steps of 610°C and 620°C were added. Possible mineralogical changes were controlled by measuring the bulk susceptibility after each step. At about 580°C, 85% of the specimens showed residual remanences which represent less than 10% of total natural remanent magnetization (*NRM*). These behaviors suggest that, once again, the main carriers of remanence are Ti-poor titanomagnetites. AF demagnetization was applied using 12 steps from 2 to 90 mT. Some specimens presented soft viscous remanences and were easily removed in fields of 5 to 15 mT.

Remanent magnetization directions were determined by the principal component analysis method (*Kirschvink, 1980*), 5 to 11 points being taken for this determination. Primary directions were averaged by site and the statistical parameters calculated assuming a Fisherian distribution (Table 1).

Characteristic remanent magnetization (*ChRM*) defined for sites 1SG to 17SG (located in the lower part of the sequence) correspond to normal polarity geomagnetic field. In general, the specimens presented unblocking temperatures under 580°C indicating that magnetite or Ti-poor titanomagnetite is the main remanence carrier. Most of these specimens have unblocking temperature spectra well above 300°C (Fig. 4a) while in some cases a minor secondary overprint (removed at low temperatures) is observed (Fig. 4b). Some lavas show the subordinate presence of hematite (3SG, 4SG, 14SG, 15SG and 16SG), with 10% of initial remanences still surviving above 580°C. These mineral phases of high unblocking temperature have RM with identical directions to those defined at

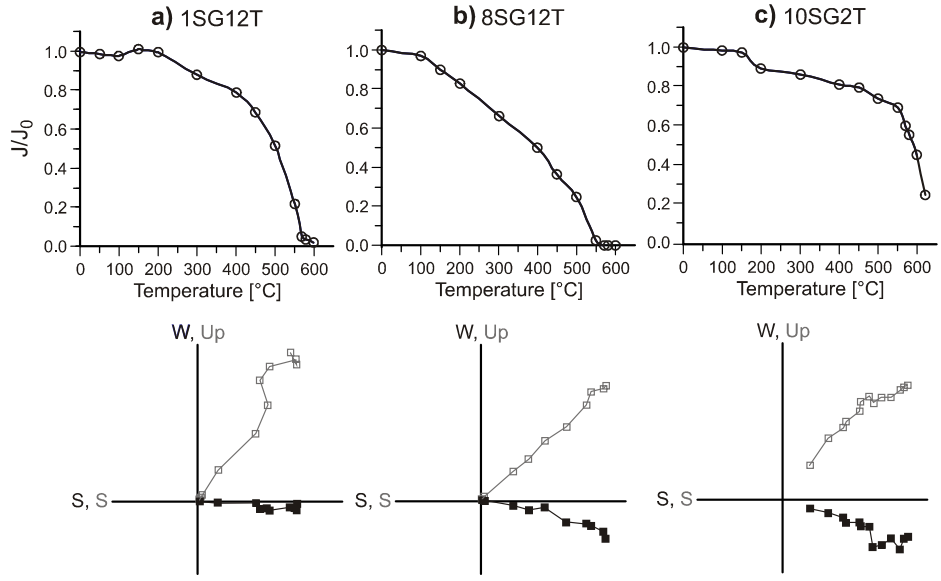

Fig. 4. Magnetic intensity curves (top) and orthogonal vector plots (bottom) of stepwise thermal demagnetization of three representative specimens. In orthogonal plots, open (solid) squares indicate projection onto the vertical (horizontal) plane.

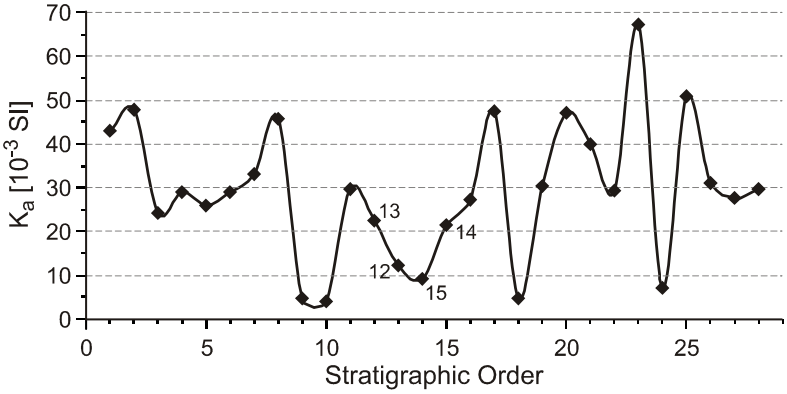

Fig. 5. Site average bulk magnetic susceptibility (K_a) for site versus stratigraphic order. Except for the sites 12 to 15, indicated in the curve, the site number corresponds to the stratigraphic order.

lower temperatures. Only in two sites (9SG and 10SG) the presence of hematite is important. Their specimens have a large range of coercivities and unblocking temperature spectra, keeping 40 to 45% of the *NRM* above 580°C (Fig. 4c). The presence of hematite is also revealed judging from their relatively low susceptibilities (Fig. 5).

The site 18SG stratigraphicaly overlies 17SG which is situated 80m below. The site-mean susceptibility (K_a) is relatively low, but the two specimens thermally demagnetized show that the remanence is not completely removed at 580° (4 to 8% of the *NRM* still remains). It is worth to note that there is no evidence of viscous remanent magnetization in these particular samples. All *ChRM*s were defined with maximum angular deviation (*MAD*) smaller than 3° corresponding to intermediate/high coercivities and reverse polarity magnetic fields.

Basalts of flow 19SG have intermediate K_a values. The AF demagnetization of 6 specimens allowed to define normal polarity components using 6 to 11steps and $MAD < 3°$. The coercivity spectra are quite large and the demagnetization curves show a typical, quasi-exponential shape, common for thick massive flows of coarse grains and high content of multidomain (MD) ferrimagnetic particles with low oxidation (*Dunlop and Özdemir, 1997*). The Zijderveld plots show rather curved lines for AF (Fig. 6a) and a complex behaviour for thermal treatment (Fig.6b). By TD, a component with similar direction to those defined by AF is removed from 50°C to 400–450° while the demagnetization curve shows a gradual increase of intensity. A second component - almost anti-parallel to the first one is removed from 450°C to 580°C. Finally, a third component yielding the almost same direction that the low temperature component is destroyed above 580°C. In this flow, unblocking temperatures of samples with positive inclination (reverse polarity) suggest that the magnetic carrier is magnetite or Ti-poor titanomagnetite. On the other hand, normal polarity components with low and high unblocking temperature could be carried by titanomaghemite and hematite, respectively. Presence of these minerals formed by low temperature oxidation has also been observed on polished section showing magnetite phenocrysts with slight alteration to hematite or in

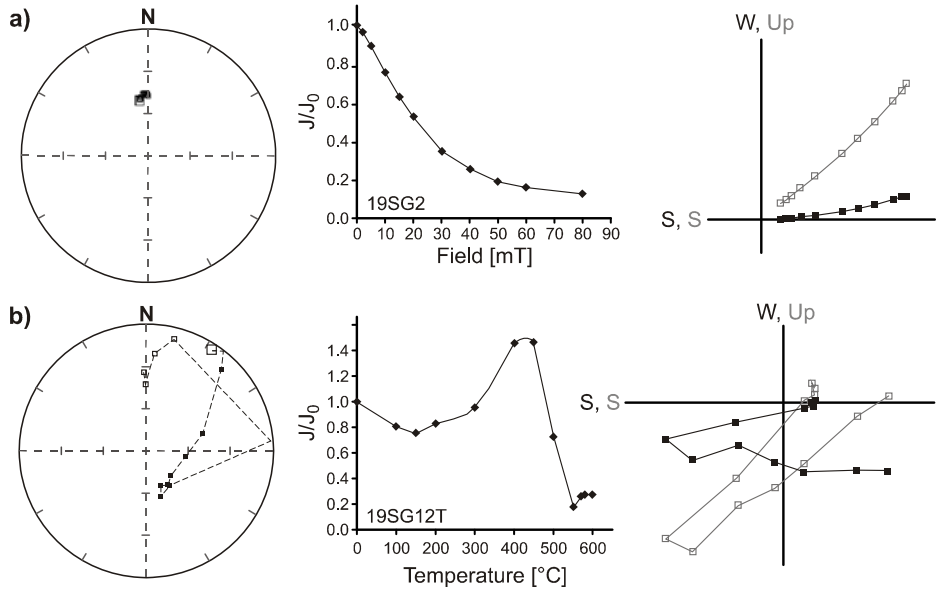

Fig. 6. Stereoplots, magnetic intensity curves and orthogonal vector plots of: **a)** stepwise alternating field, and **b)** thermal demagnetization of two representative specimens.

few cases to maghemite. Since the titanomagnetite can be considered the primary magnetic minerals of this volcanic rock, it could be assumed that the primary remanence can be represented by the reversed component defined by demagnetization at 450–580°C range. This component would not be defined by AF due to the contrast between the high maghemite and hematite and the low titanomagnetite coercivities. Fine size of particles formed by oxidation, in front of MD titanomagnetites particles, more resistant to the processes of oxidation, could contribute to this hiding. Then, the direction defined by AF would be the resultant of components defined by thermal demagnetization due to the important coercivity overlap. When the best fit great circles for the residual remanence positions obtained by AF and thermal demagnetization are calculated this hypothesis is reinforced (Fig. 7): the closed grouping of the plane poles suggest that the antipodal component is present in the specimens treated with AF demagnetization, although this process was not able to discriminate them.

The two antipodal components found may have two possible explanations:

1. Normal polarity components from site 19SG yielded directions statistically indistinguishable from the *ChRM* defined for the flow stratigraphically situated immediately above (20SG). In this case a volcanic episode younger than flow 19SG may remagnetize all magnetic particles with unblocking temperatures below 450°C or alternatively, can favor the formation of maghemite and hematite by oxidation processes which recorded the magnetic field direction corresponding to the new, normal magnetic polarity.

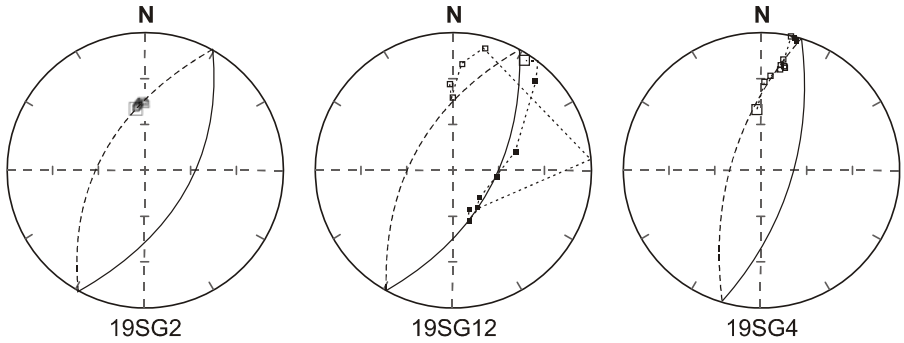

Fig. 7. Stereoplots of stepwise AF (19SG-2; 19SG-4) and thermal demagnetization (19SG-12) and best fit great circles for the residual remanence position of representative specimens from site 19SG.

2. Since the normal polarity components show directions almost anti-parallel to the reversed ones, self-reversed magnetization may have happened in hematite and maghemite. Self-reversal behavior are now well documented in some hemoilmenite-bearing igneous rocks (*Goguitchaichvili et al., 2002*). When titanohematites become ferrimagnetic during the cooling, its spontaneous magnetic moments can be oriented anti-parallel to the magnetite or titanomagnetite remanence, so that a partial self-reverse appears by magnetostatic interaction between both minerals. Self-reversed hematite occurrences are described in *Dunlop and Özdemir (1997)* and *Bina et al. (1999)* among others. On the other hand, during the basalt oxidation processes titanomagnetite can generate titanomaghemite that may carry self-reversed magnetization (*Özdemir, 1987*). *Doubrovine and Tarduno (2004)* have reported self-reversals from oceanic basalt where self-reversed magnetization is carried by titanomaghemite formed by low temperature oxidation.

On the other hand, the fact that the secondary components are statistically antipodal to the primary ones imposes little angular deviation to the primary direction, and the component defined between 450 and 580°C can be employed to characterize the flow remanence direction.

The later site (20SG) corresponds to a 3 m thick basaltic flow of similar color to the previous one, but with conspicuous columnar and horizontal disjunction, located 20 km to the east and with altitude 20 m higher than the previous flow. Its K_a is relatively high contrary to the precedent site (Fig. 5). Both AF as well as thermal demagnetization defined *ChRM* directions with normal polarity and *MAD* < 3.5°, employing from 5 to 12 steps.

*ChRM*s defined by AF or thermal demagnetization (Fig. 8a) for the two following flows (21SG and 22SG) have reverse polarity. Several specimens from these sites show disperse secondary components corresponding to normal polarities. Those components are carried by low coercivity phases that are destroyed with fields up to 15 mT and with temperatures under 200–350°C. These secondary components can be attributed to

overprint caused by later effusive episodes since the following flows carry only normal polarity remanences.

Site 23SG shows the highest K_a of the whole sequence. Using AF demagnetization, normal polarity *ChRM* with 10 to 15 steps and $MAD < 5°$ were defined after eliminating scattered viscous remanences of very low coercivities in most of the specimens. Demagnetization curves show typical exponential shapes of titanomagnetites. Two specimens carried a high coercivity component with a direction near opposite to the before mentioned *ChRM*s (Fig. 8b). Similar normal components were defined by thermal demagnetization on 4 to 8 steps and $MAD < 5°$. Their unblocking temperatures are between 450°C and 550°C. Residual components with very small intensity and nearly antiparallel to the normal direction remain above 580°C.

Sites 24SG and 25SG do not carry secondary components. In both cases, 7 to 12 steps were used to determine *ChRM* directions, giving $MAD < 4°$. While in the site 24SG *ChRM*s are carried by titanomagnetite as well as hematite, in 25SG they are carried by titanomagnetite alone. This is reflected on demagnetization curves and on relatively low Ka values for site 24SG and high for site 25SG. Specimens from site 24SG maintain around 25% of their *NRM* above 580°C.

The following three sites have intermediate K_a and carry a normal polarity primary and a near antipodal secondary components. AF and thermal demagnetization from site 26SG allowed definition of the normal component by 7 to 15 steps and $MAD < 4°$. Thermal demagnetizations showed scattered residual components with nearly opposite

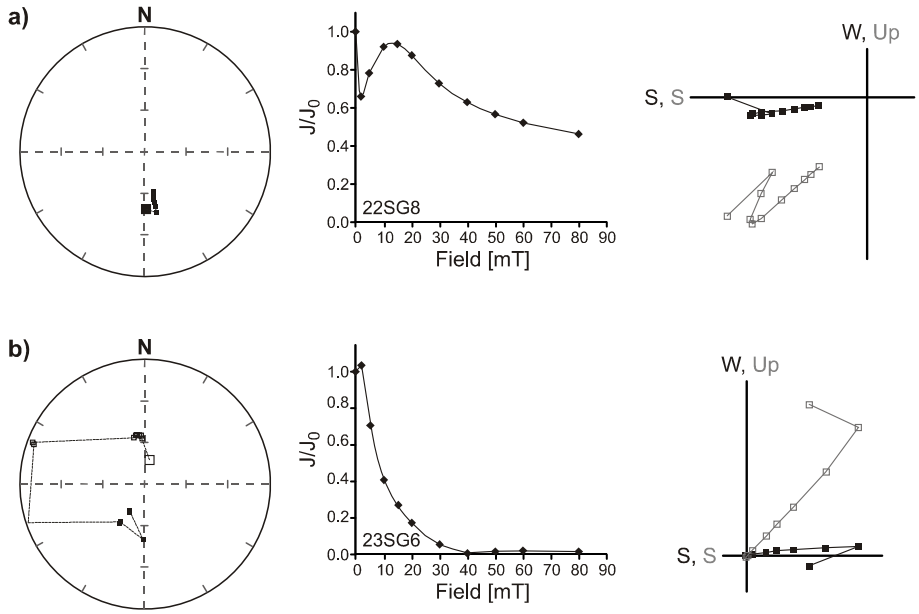

Fig. 8. Stereoplots, magnetic intensity curves and orthogonal vector plots of stepwise alternating field of two representative specimens from: **a)** 22SG and **b)** 23SG sites.

sense to the normal and only 2% of the *NRM* intensity remaining above 580°C. Thermal demagnetization for site 27SG allows to define normal components with unblocking temperatures corresponding to magnetite. There is no significant remanence above 580°C. AF demagnetization defines the same normal direction but above 80mT appears a very small intensity component near antiparallel to the first one. Finally, site 28SG presents two remanence components. The first corresponds to a normal polarity field and has coercivities under 20 mT and unblocking temperatures between 200 and 570°C. The other has an antiparallel direction being defined between 30 and 90 mT and 580 to 650°C with $MAD < 4°$ (Fig. 9a, b and c).

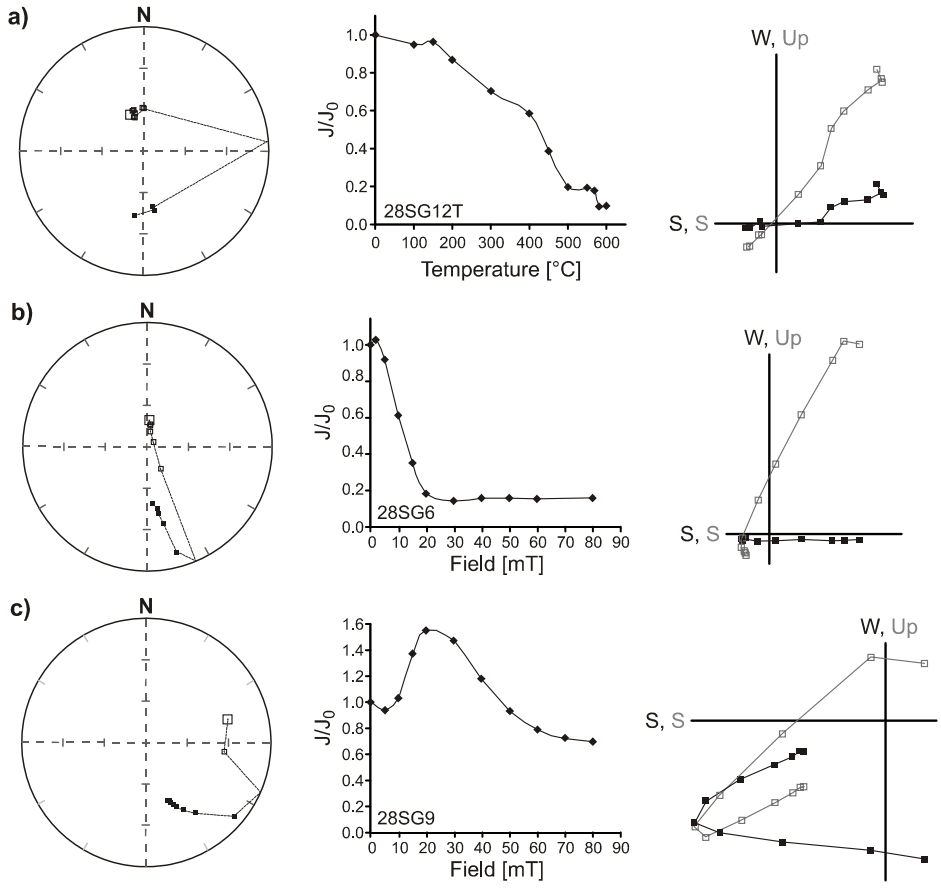

Fig. 9. Stereoplots, magnetic intensity curves and orthogonal vector plots of: **a)** stepwise thermal demagnetization, and **b)** and **c)** alternating field of of representative specimens from 28SG site.

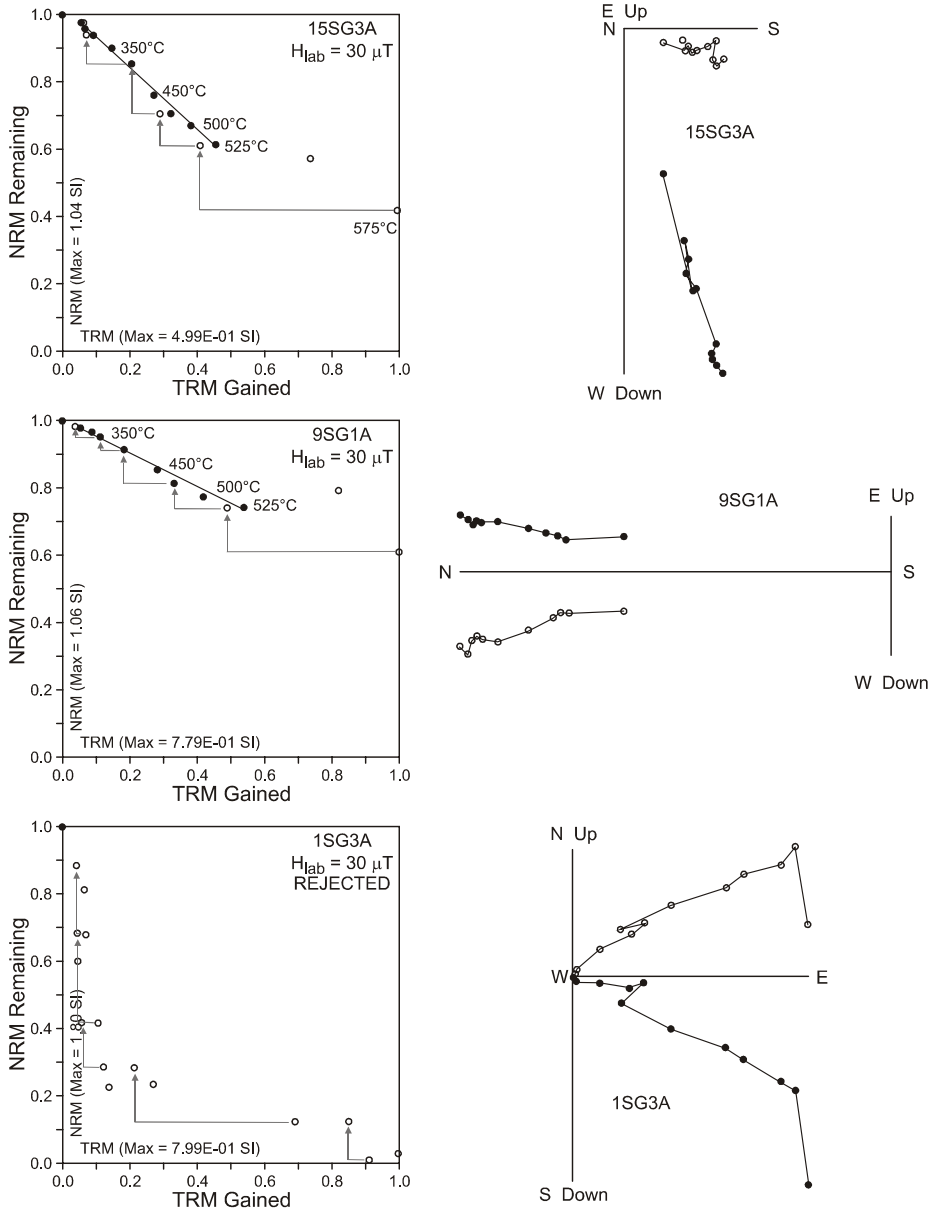

Fig. 10. The representative *NRM-TRM* plots and associated orthogonal diagrams from Posadas Formation.

5. PALEOINTENSITY DETERMINATION

Paleointensity experiments were performed using the Thellier method (*Thellier and Thellier, 1959*) in its modified form (*Coe et al., 1978*). The heatings and coolings were made in air and the laboratory field set to 30 microtesla. Ten temperature steps (*NRM*, 200°C, 250°C, 300°C, 350°C, 400°C, 450°C, 475°C, 500°C, 525°C, 550°C and 575°C) were distributed between room temperature and 575°C. The *TRM*/*NRM* checks (so-called *pTRM* checks) (*Goguitchaichvili et al., 1999*) were performed after two consecutive heating steps (Fig. 10) in order to avoid additional heatings during Thellier paleointensity experiments, which may alter significantly the magnetic carriers. So called *pTRM* tail checks are often incorporated during the measurements (*Riisager et al., 2002*) to detect the presence of multidomain magnetic grains. We prefer avoid this procedures because of additional heatings required.

Following the paleodirectional and rock-magnetic results, altogether 43 samples belonging to 9 cooling units, yielding stable, one component magnetization with blocking temperatures compatible to Ti-poor titanomagnetite phase, low viscosity index (lower than 5%) and reasonably reversible κ-T curves were selected for paleointensity experiments.

Paleointensity data are reported on the classical Arai-Nagata (*Nagata et al., 1963*) plot in Fig. 10 and results are given in Table 2. We accepted only determinations: (1) which were obtained from at least 8 *NRM-TRM* points corresponding to a *NRM* fraction larger than 1/3 (Table 2), (2) yielding quality factor (*Coe et al., 1978*) of about 5 or more, and (3) with positive '*pTRM*' checks. In most cases the linearity was observed up to 500–525°C (Fig. 10, samples 15SG3A and 9SG1A) and the control heatings were successful, i.e. the deviation of '*pTRM*' checks were less than 15%. The direction of *NRM* left at each step, obtained from the paleointensity experiments are reasonably linear and point to the origin. No deviation of *NRM* left directions towards the direction of applied laboratory field was observed. *Valet and Herrero-Bervera (2000)* and *Tauxe and Staudigel (2004)* yielded some experimental evidences that the zero field demagnetization performed prior to the *TRM* in the Coe version prevents to see the possible acquisition of chemical remanent magnetization (*CRM*). In order to monitor the potential *CRM* production, we calculated the ratio of potential *CRM*(*T*) to the magnitude of *NRM*(*T*) for each double heating step in the direction of the laboratory field during heating at *T* (*Goguitchaichvili et al., 1999*). The values of the angle between the direction on characteristic remanent magnetization (*ChRM*) obtained during the demagnetization in zero field and that of composite magnetization (equal to *NRM*(*T*) if *CRM*(*T*) is zero) are all < 6° which attest that no significant *CRM* was acquitted during the laboratory heatings.

A typical 'concave-up' behavior (*Dunlop and Özdemir, 1997*) was detected in some cases (Fig. 10, sample 1SG3A). Up to 400–450°C an important loss of *NRM* without any noticeable *TRM* acquisition but with positive *pTRM* checks is observed. This phenomenon can be due to irreversible variations of coercive force (*Kosterov and Prévot, 1998*) at low temperature and can be interpreted as transformation from a single-domain 'metastable' state to polydomain state which results in a large *NRM* lost without any correlated *TRM* acquisition during the subsequent cooling.

Table 2. Paleointensity results from Posadas Formation. n - number of point defining a straight segment on the Arai-Nagata plot; T_{min}–T_{max} is the temperature interval used for paleointensity determination; f - fraction of extrapolated *NRM* used; g - gap factor; q - quality factor; $F_E \pm \sigma(F_E)$ is individual paleointensity estimate and associated error; $F_E \pm$ s.d. means site mean and associated standard deviation; *VDM*; *VDMe* - individual and average virtual dipole moments.

Site	Sample	n	T_{min}–T_{max} [°C]	f	g	q	$F_E \pm \sigma(F_E)$ [°]	*VDM*	$F_E \pm$ s.d. [°]	*VDMe*
3SG	3SG3A	8	200–500	0.41	0.81	6.6	28.4 ± 1.3	6.37	30.1 ± 3.3	6.8 ± 0.7
	3SG4A	8	200–500	0.52	0.80	9.2	26.4 ± 1.1	5.93		
	3SG5A	9	200–525	0.47	0.82	7.3	33.4 ± 2.6	7.50		
	3SG6A	9	200–525	0.46	0.84	6.8	32.2 ± 2.3	7.23		
8SG	8SG2A	8	200–500	0.71	0.83	7.2	46.4 ± 2.1	10.1	44.0 ± 2.2	9.6 ± 0.5
	8SG3A	8	200–500	0.63	0.79	5.7	42.3 ± 1.8	9.24		
	8SG7A	8	200–500	0.59	0.83	6.7	43.2 ± 2.4	9.43		
9SG	9SG1A	9	200–525	0.32	0.84	8.6	23.6 ± 1.5	4.51	25.2 ± 2.2	4.8 ± 0.4
	9SG7A	9	200–525	0.35	0.83	6.2	26.7 ± 1.6	5.11		
15SG	15SG3A	9	200–525	0.43	0.87	17.6	45.4 ± 2.3	10.7	42.3 ± 3.1	9.9 ± 0.7
	15SG5A	9	200–525	0.45	0.81	6.6	42.4 ± 2.1	9.95		
	15SG9A	8	200–500	0.39	0.79	5.9	39.2 ± 2.0	9.20		
24SG	24SG4A	9	200–525	0.36	0.84	6.2	37.7 ± 2.3	7.91	34.9 ± 2.5	7.3 ± 0.5
	24SG5A	8	200–500	0.31	0.78	5.5	33.3 ± 1.8	6.99		
	24SG7A	8	200–500	0.37	0.78	6.4	33.6 ± 1.6	7.05		

6. MAIN RESULTS AND DISCUSSION

6.1. Paleodirecions and Magnetic Polarities

The average flow directions are rather precisely determined for 26 out of 28 sites (Table 1) with α_{95} (twice the standard error of the mean) less than 10° which points to small within-site dispersion and high directional stability. The other two sites have α_{95} of 10.4° and 15.3°. Twenty four sites give normal polarity primary magnetization and four have reverse primary magnetization. One of the reversely magnetized site presents a single component. Few samples from the other sites show reverse polarity magnetizations carried by (titano)magnetites, while hematites and probably maghemites carry opposite paleodirections probably due to self-reversed magnetization. On the other hand, few samples from another three sites show a opposite behavior with normal polarity magnetizations carried by (titano)magnetites, and hematites and maghemites with almost antipodal directions. Because (titano)magnetites are primary minerals, we believe thus that they carry primary remanent magnetizations. Under this hypothesis, the volcanic sequence studied here, presents at least two polarity reversals. The occurrence of reverse and normal polarities in Parana Lavas were already detected by *Ernesto et al. (1990)* and

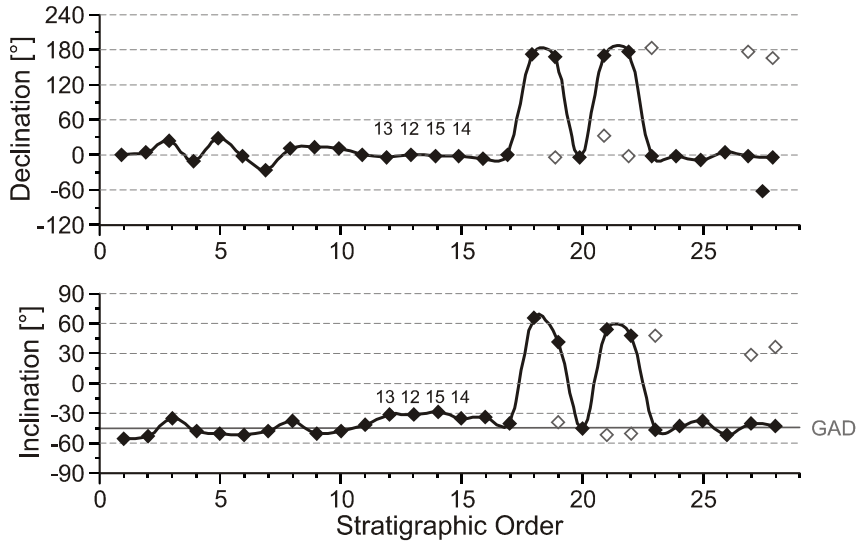

Fig. 11. Changes in declination and inclination of the site mean directions on stratigraphic order. Secondary directions are shown as empty grey diamonds. The solid grey line indicates the GAD field position for the sites.

have been seen by several authors later (*Alva-Valdivia et al., 2003*; *Mena et al., 2006* among others). Fig. 11 shows the variations in declination (D) and inclination (I) of the site mean directions while corresponding virtual geomagnetic poles (VGP) with their Fisherian parameters are shown in Table 1.

The sequence of paleodirections in stratigraphic order shows that the first flows cooled down during periods of normal polarity geomagnetic field (flows 1SG to 17SG). The two following flows (18SG and 19SG) recorded an interval of reverse polarity, while the 20SG flow showed a normal polarity. Sites 21SG and 22SG also yielded a reverse polarity. Finally the 23SG to 28SG flows have *ChRM*s corresponding to normal magnetic polarity. From these considerations it may be suggested that the effusive sequence recorded at least two polarity reversal (N-R-N). If the hypothesis that flow 20SG is younger than 19SG is valid, then the sequence would record four changes of polarity (N-R-N-R-N). It worth noting that the lava flow sequence reported in *Mena et al. (2006)* corresponding to the 6 to 28 new sites, show normal remanences in the bottom and top flows and reverse polarities in the middle.

The mean paleomagnetic direction of normal polarity sites is $I = -42.9°$, $D = 0.3°$, $k = 53.7$, $\alpha_{95} = 4.2°$, $N = 23$ (k is precision parameter and N number of sites) while reversely magnetized sites give $I = 55.9°$, $D = 174.1°$, $k = 69.8$, $\alpha_{95} = 14.9°$, $N = 3$. The reversal tests as defined by *McFadden and Lowes* (1981) and *McFadden and McElhinny (1990)* are both rejected at the 95% confidence level ($\gamma_c = 12.12°$; $\gamma_o = 13.60°$). In fact the first test is not strictly valid because one of the distributions has less than 5 data, but the second is valid because statistically at 95% level have a common k parameter

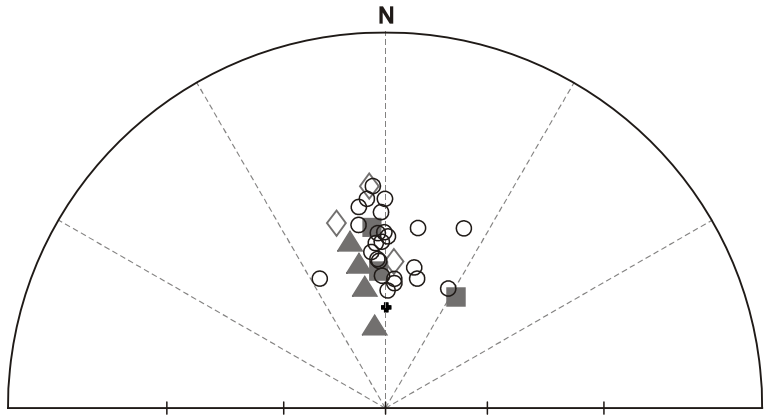

Fig. 12. Stereoplots for site mean direction corresponding to normal polarity (black circles), antipodal directions to site mean corresponding to reverse polarity (grey full triangles), mean secondary directions with normal polarity (grey full squares) and antipodal of mean secondary directions with reverse polarities (diamonds).

(k_r/k_n = 1.2990; $F_{44;4;0.05}$ = 5.7091). Notably, when mean site secondary directions are also considered (Fig. 12), both reversal tests are accepted at 95% confidence level (γ_c = 8.85°; γ_o = 6.13°, type B; k_n/k_r = 1.2391; $F_{12;52;0.05}$ = 1.9436).

The distribution of the site-mean VGPs is somewhat elongated (Fig. 13). Similar configuration was also found for coeval VGPs (*Mena et al., 2006*). However, the elongation is not significant since the VGP distribution yields a reasonably good fit with fisherian distribution when probability plots as well as formal testing procedures are used. The quantil-quantil (Q-Q) plot for longitudes using the uniform model is approximately linear, passing through the origin with a slope near 45° (Fig. 14a). The Q-Q colatitude plot with exponential model is also linear (Fig. 14b), with a slope that gives an estimated k = 42.92. In this plot four points could be considered outliers with respect to the fisherian model (3SG, 5SG, 7SG, 18SG). In other hand, considering the sample size, these outliers can be attributed to fluctuation due solely to sampling variability. The new slope calculated without these points give a k = 67.57. The Q-Q plot for two variables (Fig. 14c) is approximately linear, passing through the origin and with a slope that give an estimate k = 47.56. The three k estimate values are statistically undistinguishable at 95% level using an F-test. The fact that estimates of k with colatitude and two variables tests are in reasonable agreement suggests that the underlying distribution is fisherian. Employing formal testing procedures, we obtain the following results for the modified statistics of Kolmogorov-Smirnov and Kuiper (D_n^*, V_n^*, $M_U\left(V_n\right)$, $M_E\left(D_n\right)$ and $M_N\left(D_n\right)$; *Fisher et al., 1987*): Longitude test: $D_n^* = 0.673$; $V_n^* = 1.134$; $M_U\left(V_n\right) = 1.038$; colatitude test: $D_n^* = 1.11$; $V_n^* = 1.743$; $M_E\left(D_n\right) = 1.114$; Two-variable test: $D_n^* = 0.608$; $V_n^* = 1.063$; $M_N\left(D_n\right) = 0.609$. The significance probability exceeds 10% for longitude and two-

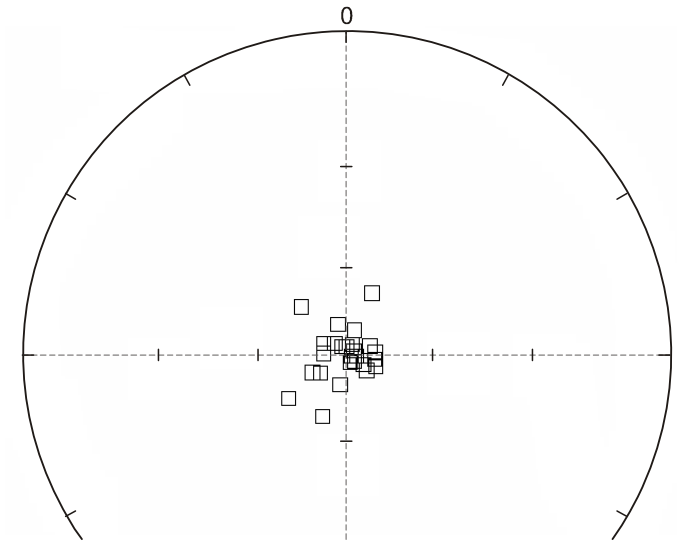

Fig. 13. South VGPs distribution from 26 sites with $\alpha_{95} < 10°$.

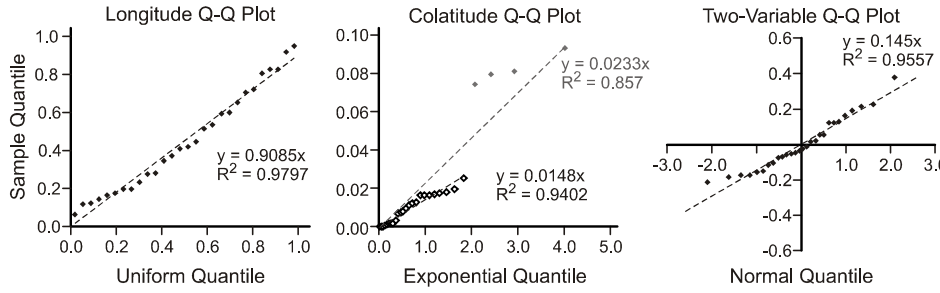

Fig. 14. Probability plots for checking goodness of fit of the VGPs to the Fisher distribution.

variable statistics, but for the colatitude test this only happens with D_n^* while V_n^* significance probability exceeds 5% and $M_E(D_n)$ statistic lies between the 5% and 1% points, suggesting some small departure from the Fisher model.

Considering the PGVs from sites with $\alpha_{95} < 10°$ the paleomagnetic pole (PP) is located at 339.1° longitude E, 89.7° latitude S, $N = 26$, $K = 45.6$, $A_{95} = 4.2$.

6.2. Paleosecular Variation

Statistical models of paleosecular variation (PSV) predict that the dispersion in VGPs tends to increase with site paleolatitude. VGPs scatter is commonly calculated with the total angular dispersion (S_p) according to *Cox (1969)*:

$$S_p^2 = \sum_{i=1}^{N} \Delta_i^2 \big/ (N-1),$$

where N is number of sites used in the calculation, Δ_i is angular distance of the i-th VGP from the axial dipole.

Since our calculated PP is nearly coincident whit the present-day Earth spin axis, the last was used to calculate VGP angular deviations (Δ) (Table 3). This way, S_p = 12.1°. It is interesting that the Δ for the discarded sites (with $\alpha_{95} > 10°$) has not significantly larger deviations.

Table 3. Paleosecular variation results. Δ is VGP angular deviation from geographic pole; K means Fisher concentration parameters for VGPs, S_w is within-site scatter; n numbers of directions used; $\Delta^2 - S_w^2/n_i$ represents corresponding difference involved in the calculation of the corrected total angular dispersion S_p. The discarded sites (with $\alpha_{95} > 10°$) are indicated in italics and the negative differences are emphasized in bold.

Site	Δ	K	S_w	N	$\Delta^2 - S_w^2/n_i$
1	8.7	49.97	11.5	9	61.10
2	7.6	406.43	4.0	10	56.15
3	22.7	78.45	9.1	8	504.84
4	9.5	87.28	8.7	7	79.51
5	24.6	81.75	9.0	8	595.13
6	5.7	321.26	4.5	7	29.57
7	23.6	315.04	4.6	6	553.49
8	10.5	46.96	11.8	9	94.73
9	12.9	152.06	6.6	8	161.02
10	10.6	270.14	4.9	5	107.50
11	3.0	230.78	5.3	8	5.45
13	10.4	288.22	4.8	6	104.37
12	9.1	101.11	8.1	10	76.32
15	11.3	74.45	9.4	5	110.06
14	7.2	336.89	4.4	9	49.68
16	10.6	223.23	5.4	8	108.69
17	3.8	361.85	4.3	5	10.81
18	22.8	77.88	9.2	6	505.80
19	*11.1*	*239.01*	*5.2*	*2*	*109.48*
20	4.7	47.59	11.7	6	**–0.89**
21	11.3	41.46	12.6	8	107.91
22	3.3	200.54	5.7	8	6.80
23	3.2	230.55	5.3	5	4.55
24	2.1	238.00	5.3	7	0.47
25	9.3	106.81	7.8	6	76.25
26	*7.3*	*26.19*	*15.8*	*8*	*21.98*
27	4.0	45.34	12.0	8	**–2.09**
28	3.5	49.78	11.5	11	0.27

S_p will be partly caused by the geomagnetic secular variation and partly by random errors associated with rock heterogeneities and sampling and measuring processes. To remove the later source *McEllhinny and McFadden (1997)* defined the parameter S_B

$$S_B^2 = \sum_{i=1}^{N} \left(\Delta_i^2 - S_{w_i}^2 \Big/ n_i \right) \Big/ (N-1) ,$$

where S_w is the within-site scatter, calculated as $S_w = 81/\sqrt{K}$; K being Fisher concentration parameter for poles estimate from direction concentration parameter (k) according to $K = 8k \Big/ \left(5 + 18\sin^2 \lambda + 9\sin^4 \lambda \right)$, with λ site paleolatitude (*Cox, 1970*), and n_i number of directions from i-th site .

To calculate secular variation parameters the current average site latitude ($\lambda = 26.5$ºS) was employed as site paleolatitude. The results are shown in Table 3. When the within-site scatter corrections were negative they were considered equal to zero. This way, $S_B = 11.68$º, with lower and upper 95% confidence limits of 9.8º and 14.5º respectively, calculated according to $2(N-1)S^2 / \sigma^2 \sim \chi^2_{2(N-1)}$. These VGP dispersion is smaller than the expected value for this latitude (≈ 14°) according to the curve for 0–5 Ma lapse from *McElhinny and McFadden (1997)*. On the other hand, if the S_B is compared with the calculated for *Johnson et al. (2008)*, the value here obtained is significantly smaller that the VGP dispersion for Matuyama chron and for 0–5 Ma time interval for sampling latitude band, 10º wide, centered on 22.1°S, but that value is included in the 95% confidence intervals from Brunhes chron for 22.1°S and 27.1°S centered bands.

Biggin et al. (2008) analyzed the PSV from a VGP database of CNS (84–125 Ma) and Jurassic ages (145–200 Ma), (their Group 2) and a subconjunct of higher quality data (their Group 1, $n > 5$; $k > 50$). These authors used the Model G (*McFadden et al., 1988*) to describe the shapes of the curves that predict average VGP scatter as a function of latitude according to $S_B^2 = a^2 + (b\lambda)^2$, where a and b are the antisymetric and symetric family coefficients. Employing the a, b best fit values from *Biggin et al. (2008)* and the site paleolatitude the expected mean and confidence intervals were estimated (Table 4). The S_B values here obtained agree well with the selected data reported for the Cretaceous Normal Superchron. A similar comparison with the Jurassic data is quite delicate due to the limitation of paleolatitudinal span and relatively poor quality of available data. Thus, our data reinforces the hypothesis outlined by *Biggin et al. (2008)* about the different style of secular variation during (and before) CNS and Plio-Quaternary times supporting the link between PSV and reversal frequency.

The location of our new PP (1-MIS, Fig. 15, Table 5), is very near to the Earth spin axis. This PP is statistically indistinguishable from the Florianopolis PP (*Raposo et al., 1998*) and the mid-Cretaceous mean-poles (125–100 Ma) for South America, calculated by *Somoza and Zaffarana (2008)*, (PPs 9, 14 and 15, Fig. 15). The 1-MIS PP agrees with PPs of similar and younger ages from the Central Paraná Magmatic Province (132–133 Ma; *Alva-Valdivia et al., 2003*), Central Alkaline Province, Paraguay

Table 4. Angular dispersion of VGPs. *a*, *b* are shape parameters calculated from *Biggin et al. (2008)*, by data from their Group 1 and 2 (more details in text); S_B - angular dispersion of VGPs due to PSV calculate according to Model G of *McFadden et al. (1988)*. CNS - Cretaceous Normal Superchron; *mean, low. l, up. l*. are mean, lower and upper confidence limits for the *a*, *b*, parameters and S_B values calculated using this values.

a, *b* (from *Biggin et al., 2008*)							$\lambda = 26.5$
		Group 1			Group 2		
		a	*b*	S_B	*a*	*b*	S_B
CNS	*low. l.*	6.3	0.22	8.58	7.8	0.22	9.74
	mean	8.7	0.27	11.26	9.9	0.26	12.06
	up. l.	10.7	0.31	13.49	11.3	0.29	13.67
Jurassic	*low. l.*	10.3	0	10.30	8.3	0.14	9.09
	mean	16.4	0.19	17.16	10.8	0.24	12.53
	up. l	19	0.46	22.57	12	0.32	14.69

(127–130 Ma; *Ernesto et al., 1996*), Sierras Pampeanas (~130 Ma; *Geuna and Vizán, 1998*), Baqueró Group (~119 Ma; *Somoza et al., 2005*) and Los Adobes Formation (112–130 Ma; *Geuna et al*., 2000), (PPs 6, 7, 8, 10 and 11, Table 5, Fig. 15). 1-MIS PP confidence region has a small overlap with the Central Paraná Basin pole and the early-Cretaceous mean-poles (135–130 Ma; *Somoza and Zaffarana, 2008*) and with the PP recently reported from coeval basalts of the Arapey formation, Uruguay (*Solano et al, 2010*), but does not agree with the Southern Paraná Basin nor with the Northern Paraná Basin poles (*Raposo and Ernesto, 1995*; *Ernesto et al., 1999*). The 1-MIS PP pole is significantly different from the pole position suggested by hotspot reconstructions (76.7°S, 116.4°E, ~130 Ma; *Muller et al., 1993*).

To analyze if the scarce overlap between our PP with the Central Paraná Province PP could be caused by incomplete average-out of the PSV, a non-parametric test for VGP serial correlation was performed. According to *Biggin et al. (2008)* the average of angular distances between the mean paleomagnetic direction of each flow and its successor ($\Delta_{i,i+1}$) were calculated ($\Delta_a = 34.29°$). The same calculus was repeated 10000 times for directions in random order. The pseudo-sample distribution have a median of 51.54° and a 5-percentile of 36.75. The Non-Random-Ordering (NRO) factor is 0.97, therefore the serial correlation can be considered significant at the 95% confidence level.

On the base of this correlation the sequential localization of VGP was analyzed. Considering that the geomagnetic field oscillates around the direction expected from a GAD field and that each VGP records an instantaneous reading of the Earth Magnetic Field, we calculated sequential moving axial averages of VGPs. For VGPs corresponding to reverse polarity, the antipodal location was considered. Windows of 5 VGPs and steps of one were used. In this way, the first average corresponds to VGPs from 1SG to 4SG sites, the second for 2SG to 5SG, and so on. Should be considered that the averages represent different and unknown time intervals.

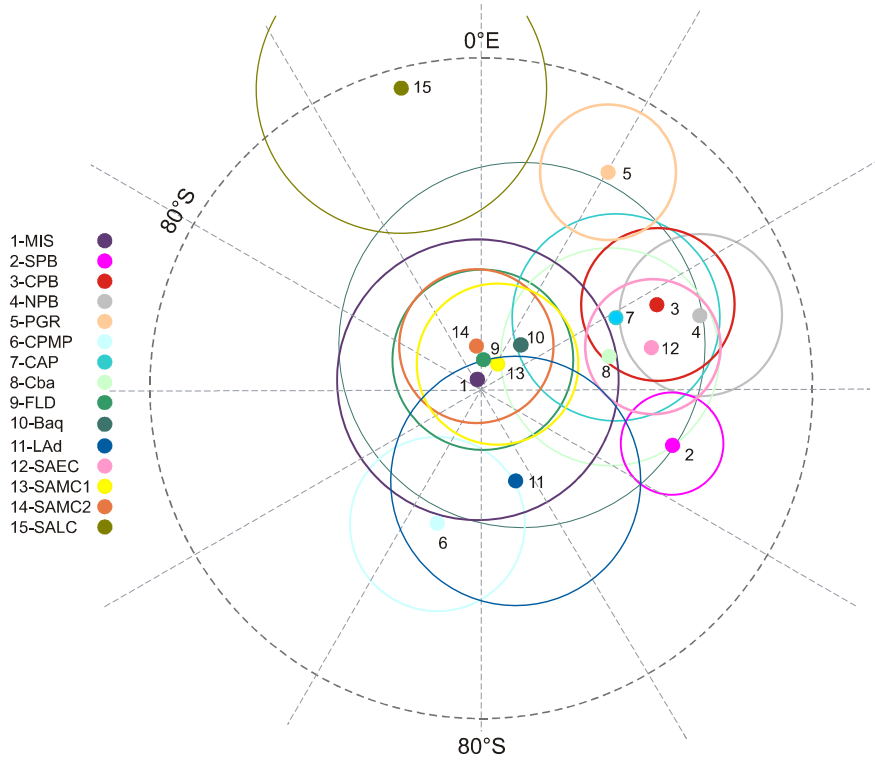

Fig. 15. Paleomagnetic poles whit 95% confidence circles for Posadas Formation and previous cretaceous PPs (Table 5).

Fig. 16 shows the sequential locations of these averages together with the PPs before considered. Interestingly the axial average VGP path traces an almost complete cycle around the geographical pole. If it is considered that the region suffered little drift from the moment when these basalts were extruded, the paleo-position of the geographical pole should have been very near to the current one. Axial average VGP path passes near the location of all Serra Geral Poles (CPM; SPB, CPB, NPB, PGR).

Taking as primary assumptions that the magnetic field, when averaged over sufficient time, is in agreement with a GAD field, then if VGPs are averaged from rocks spanning enough time to average out secular variation, the mean pole is coincident with the spin axis. But it is not very well known exactly how much time must elapse and what is the minimum number of sites required to average out completely secular variation. Magnitude of contribution of long term non dipole sources are poorly known for the age of the study rocks. It remains to be investigated whether the previous PP from the PMP completely averaged out the paleosecular variation due to uneven distribution of sampling of the paleomagnetic field as a consequence of the instantaneous and aperiodic character of the volcanic flows.

6.3. Paleointensity

Only 15 samples, coming from 5 individual basaltic lava flows, yielded acceptable paleointensity estimates. The *Thellier and Thellier (1959)* method of geomagnetic absolute intensity determination, which is considered the most reliable one, imposes many restrictions on the choice of samples that can be used for a successful determination. In particular, multi-domain magnetic grains may sometimes overestimate the absolute paleointensity (*Biggin et al., 2010*). For these samples the *NRM* fraction *f* used for determination ranges between 0.32 to 0.71 and the quality factor *q* from 5.5 to 17.6 being generally greater than 5. Although our results are not numerous, some credit should be given because of good technical quality determination, attested by the reasonably high quality factors of *Coe et al. (1978)*. The site mean palaeointensities are ranging from 25.2 ± 2.2 to 44.0 ± 2.2 μT. The *VDM*s are ranging from 4.8 to 9.9×10^{22} Am^2, values that agree with the coeval ones shown in *Tauxe and Staudigel (2004)*. This corresponds to a mean value of $7.7 \pm 2.1 \times 10^{22}$ Am^2, almost 96% of the present day geomagnetic field strength. The mean paleointensities value obtained from the Posadas Formation agree reasonably well, within the uncertainties, with those retrieved from the coeval Arapey (Uruguay) and Serra Geral (Southern Brazil) Formations (*Goguitchaichvili et al., 2008*).

Table 5. Selected Cretaceous paleomagnetic poles. *P* - number assigned to paleomagnetic pole (PP) (Figs. 15 and 16); A_{95} is semi angle of 95% confidence of the PPs.

Locality	*P*	Long. [°E]	Lat. [°S]	A_{95}	Age [Ma]	Reference
MIS: Misiones	1	339.1	89.7	4.2	?	This study
SPB: Southern Parana Basin	2	106.2	84	1.5	~133	*Raposo and Ernesto (1995)*
CPB: Central Parana Basin	3	64.4	84.1	2.3	~132	*Raposo and Ernesto (1995)*
NPB: Northern Parana Basin	4	71.4	83	2.4	132	*Ernesto et al. (1999)*
PGR: Ponta Grossa dikes (Brazil)	5	30.3	82.4	2	129–131	*Raposo and Ernesto (1995)*
CPMP: Central Parana Magmatic Province, Brazil	6	197.9	85.7	2.6	132–133	*Alva-Valdivia et al. (2003)*
CAP: Central Alkaline Province, Paraguay	7	62.3	85.4	3.1	127–130	*Ernesto et al. (1996)*
Cba: Sierras Pampeanas, Cordoba	8	75.9	86	3.3	~130	*Geuna and Vizán (1998)*
FLD: Florianopolis dikes, Southern Brazil	9	3.3	89.1	2.7	119–128	*Raposo et al. (1998)*
Baq: Baqueró Group	10	42.7	88.2	5.5	119	*Somoza et al. (2005)*
LAd: Fm. Los adobes	11	159	87	3.8	112–130	*Geuna et al. (2000)*
SAEC: Mean South America Early Cretaceous	12	76.4	84.7	2	135–130	*Somoza and Zaffarana (2008)*
SAMC1: Mean S.A. Mid-Cretaceous	13	33.8	89.1	2.4	125–100	*Somoza and Zaffarana (2008)*
SAMC2: Mean S:A: Mid-Cretaceous	14	354.1	88.7	2.3	125–100	*Somoza and Zaffarana (2008)*
SALC: Mean S.A. Late Cretaceous	15	345.1	80.6	4.3	85–65	*Somoza and Zaffarana (2008)*

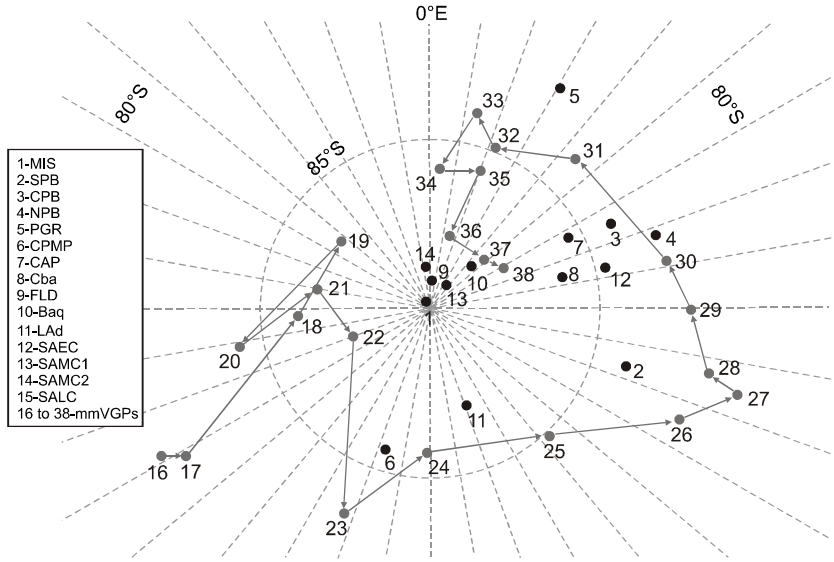

Fig. 16. Location at South hemisphere of selected paleomagnetic poles (blue, Table 5) and path of sequential mean VGPs calculated using moving averages (mmVGPs).

The slightly older Ponta Grossa dikes however, yielded relatively low geomagnetic field strength. The general characteristic of all Parana paleointensity studies is a relatively high scatter similar to findings of *Granot et al. (2007)*. Globally, early Cretaceous paleointensities appear similar to the Brunhes data. This reinforces some previous suggestions (*Goguitchaichvili et al*., *2002, 2008*) about the invalidity of the Mezozoic Dipole Low hypothesis (*Prévot et al., 1990*). High geomagnetic intensities have been reported (*Tarduno et al., 2001, 2002*) for Early Cretaceous, which are consistent with some inferences from computer simulations (*Glatzmaier et al., 1999*).

7. CONCLUSIONS

The studied samples show low capacity to acquire viscous remanent magnetizations. Low-field susceptibility measurements (κ-T curves) under air, IRM acquisition curves and AF and thermal stepwise demagnetizations indicate that magnetite or Ti-poor titanomagnetite is the main remanence carrier. Some sites show the subordinate presence of hematite or titanomaghemite. Presence of these minerals formed by low temperature oxidation has also been observed on polished sections that show magnetite phenocrysts with light alteration to hematite and in few cases to maghemite.

Primary remanent magnetizations were determined for all studied sites using both alternating field and thermal demagnetizations. Some sites yielded evidence for secondary components carried by hematite and/or maghemite showing opposite magnetic polarity. These components can be due to secondary formation of these minerals caused by low

temperature oxidation after emplacement of these lavas. Alternatively, a self-reversal phenomena of thermoremanent magnetization may be involved.

The sites showed small within-site dispersion and high directional stability. Average flow direction were precisely determined for 26 sites whit $\alpha_{95} < 10°$. The flow sequence studied has recorded at least three polarity intervals. The corresponding VGPs statistically fit with a fisherian distribution yielding significant serial correlation (NRO factor of 0.97).

A new Early Cretaceous paleomagnetic pole (PP) (339.1°E, 89.7°S, $N = 26$, $K = 45.6$, $A_{95} = 4.2$) was obtained. This PP is in agreement with other reliable early cretaceous PPs from South America but disagree with the Southern and Northern Paraná Basin poles previousely published. Although these rocks are of very similar ages, considering the sporadic nature of the eruptions, they may have not been emplaced simultaneously and therefore might have recorded different secular variation cycles.

Moving window averages each 5 VGPs were used to analyze the sequential variation of VGPs. Interestingly, the axial average VGP path traces an almost complete cycle around the geographical pole and passes near the location of all published Serra Geral paleomagnetic poles. This path includes at least two reversals and thus it could be considered an apparent or true polar wander path (PWP). Since each point of the curve represents the average dipolar position from five VGPs, they may average itself the SV of smaller duration than the time involved in the interval defined by these virtual geomagnetic poles. Both paleomagnetic pole as well as the axial average VGP path are significantly different from the pole position suggested by fixed hotspot reconstructions, which may be due to true polar wander or the hotspot motion itself.

The VGP dispersion (S_B) is smaller than the expected value for this latitude for 0–5 Ma lapse (*McElhinny and McFadden, 1997*; *Johnson et al., 2008*) but agrees well with that calculated for the Brunhes chron (*Johnson et al., 2008*) and for the Cretaceous Normal Superchron (*Biggin et al*., *2008*).

The mean *VDM*s ($7.7 \pm 2.1 \times 10^{22}$ Am^2) is almost 96% of the present day geomagnetic field strength. The Posadas Formation mean paleointensity agrees reasonably well with values from the coeval Arapey and Serra Geral Formations (*Goguitchaichvili et al., 2008*) while the slightly older Ponta Grossa dikes yielded relatively lower geomagnetic field strength. This suggests high geomagnetic intensities for the Early Cretaceous reinforcing some previous suggestions (*Goguitchaichvili et al., 2002, 2008*) about the invalidity of the Mezozoic Dipole Low hypothesis (*Prévot et al., 1990*).

References

Alva-Valdivia L.M., Goguitchaichvili A., Urrutia-Fucugauchi J., Riisager J., Riisager P. and Ferreira-Lopes O., 2003. Paleomagnetic poles and paleosecular variation of basalts from Parana Magmatic Province, Brazil: geomagnetic and geodynamic implications. *Phys. Earth Planet. Inter.*, **138**, 183–196.

Biggin A.J., 2010. Are systematic differences between thermal and microwave Thellier-type palaeointensity estimates a consequence of multidomain bias in the thermal results? *Phys. Earth Planet. Inter.*, **180**, 16–40.

Biggin A.J., van Hinsbergen D.J., Langerais C.G, Straathof G.B. and Deenen M.H.L., 2008. Geomagnetic secular variation in the Cretaceous Normal Superchron and in the Jurassic. *Phys. Earth Planet. Inter.*, **169**, 3–19.

Bina M., Tanguy J.C., Hoffman V., Prévot M., Listanco E.L., Keller R., Fehr K.T., Goguitchaichvili A.T. and Punongbayan R.S., 1999. A detailed magnetic and mineralogical study of selfreversed dacitic pumices from the 1991 Pinatubo eruption (Philippines). *Geophys. J. Int.*, **138**, 159–178.

Cande S.C. and Kent D.V., 1995. Revised calibration of the geomagnetic polarity time scale for the Late Cretaceous and Cenozoic. *J. Geophys. Res.*, **100**, 6093–6095.

Coe R., Grommé S. and Mankinen E.A., 1978. Geomagnetic paleointensities from radiocarbon-dated lava flows on Hawaii and the question of the Pacific nondipole low. *J. Geophys. Res.*, **83**, 1740–1756.

Courtillot V. and Besse J., 1987. Magnetic field reversals, polar wander, and core-mantle coupling. *Science*, **237**, 1140–1147.

Cox A., 1969. Research note: Confidence limits for the precision parameter, K. *Geophys. J. R. Astron. Soc.*, **17**, 545–549.

Cox A., 1970. Latitude dependence of the angular dispersion of the geomagnetic field. *Geophys. J. R. Astron. Soc.*, **20**, 253–269.

Day R., Fuller M.D. and Schmidt V.A., 1977. Hysteresis properties of titanomagnetites: grain size and composition dependence. *Phys. Earth Planet. Inter.*, **13**, 260–267.

Doubrovine P.V. and Tarduno J.A., 2004. Self-reversed magnetization carried by titanomaghemite in oceanic basalts. *Earth Planet. Sci. Lett.*, **222**, 959–969.

Dunlop D.J., 2002. Theory and application of the Day plot (Mrs/Ms versus Hcr/Hc), Theoretical curves and tests using titanomagnetite data. *J. Geophys. Res.*, **107**, DOI: 10.1029 /2001JB000486.

Dunlop D.J. and Özdemir O., 1997. *Rock Magnetism, Fundamentals and Frontiers*. Cambridge University Press, Cambridge, U.K., 573 pp.

Ernesto M., Pacca I.G., Hyodo F.Y. and Nardy A.J.R., 1990. Paleomagnetism of the Mesozoic Serra Geral formation, southern Brazil. *Phys. Earth Planet. Inter.*, **64**, 153–175.

Ernesto M., Comin-Chiaramonti P., Gomes C.B., Castillo A.M. and Velazquez J.C., 1996. Palaeomagnetic data from the Central Alkaline Province, Eastern Paraguay. In: Gomes C.B. and Comin-Chiaramonti P. (Eds.), *Alkaline Magmatism in Central-Eastern Paraguay*. EDUSP/FAPESP, Sao Paulo, Brazil, 85–102.

Ernesto M., Raposo I.B., Marques L., Renne P., Diogo L. and Min M., 1999. Paleomagnetism, geochemistry and 40Ar/39Ar dating of the Northeastern Paraná Magmatic Province. *J. Geodyn.*, **28**, 321–340.

Evans M.E. and Heller F., 2003. *Environmental Magnetism. Principles and applications of Environmagnetics*. Academic Press, Elsevier Science, 300 pp.

Fisher N.I., Lewis T and Embleton B.J.J., 1987. *Statistical Analysis of Spherical Data.* Cambridge University Press, Cambridge, U.K., 330 pp.

Gentili C. and Rimoldi H., 1980. Mesopotamia. *Segundo Simposio de Geología Regional Argentina, Córdoba, Vol.1.* Academia Nacional de Ciencias, Cordoba, Argentina, 185–223.

Geuna S.E. and Vizán H., 1998. New Early Cretaceous paleomagnetic pole from Córdoba province, (Argentine): revision of previous studies and implications for the South American database. *Geophys. J. Int*., **135**, 1085–1100.

Geuna S.E, Somoza R., Vizán H., Figari E.G. and Rinaldi C.A., 2000. Paleomagnetism of Jurassic and Cretaceous rocks in Central Patagonia: a key to constrain the timing of rotations during the breakup of southwestern Gondwana? *Earth Planet. Sci. Lett.*, **181**, 145–160.

Glatzmaier G.A. and Roberts P.H., 1995. A three-dimensional self-consistent computer simulation of the geomagnetic field reversal. *Nature*, **377**, 203–209.

Glatzmaier G.A., Coe R.S., Hongre L. and Roberts P.H., 1999. The role of the Earth's mantle in controlling the frequency of geomagnetic reversals. *Nature*, **401**, 885–890.

Goguitchaichvili A. and Prévot M., 2000. Magnetism of oriented single crystals of hemoilmenite with selfreversed thermoremanent magnetization. *J. Geophys. Res.*, **105**, 2761–2780.

Goguitchaichvili A., Prévot M., Roberts N. and Thompson J., 1999. An attempt to determine the absolute geomagnetic field intensity in Southwestern Iceland during the Gauss-Matyama reversal. *Phys. Earth Planet. Inter.*, **115**, 53–66.

Goguitchaichvili A., Chauvin A., Roperch P., Prévot M., Aguirre L. and Vergara M., 2000. Palaeomagnetism of the Miocene Farellones formation (Chile). *Geophys. J. Int.*, **140**, 357–373.

Goguitchaichvili A., Alva-Valdivia L., Urrutia-Fucugauchi J., Morales J. and Ferreira-Lopes O., 2002. On the reliability of Mesozoic dipole low: new absolute paleointensity results from Parana Flood Basalts (Brazil). *Geophys. Res. Lett.*, **29**, 1655, DOI: 10.1029/2002GL015242.

Goguitchaichvili A., Cejudo Ruiz R., Sanchez Bettucci L., Aguilar Reyes B., Alva-Valdivia L.M., Urrutia-Fucugauchi J., Morales J. and Calvo Rathert M., 2008. New absolute paleointensity results from the Parana Magmatic Province (Uruguay) and the Early Cretaceous geomagnetic paleofield. *Geochem. Geophys. Geosyst.*, **9**, Q11008, DOI: 10.1029/2008GC002102.

Granot R., Tauxe L., Gee J.S. and Ron H.A., 2007. View into the Cretaceous geomagnetic field from analysis of gabbros and submarine glasses. *Earth Planet. Sci. Lett.*, **256**, 1–11.

Gubbins D., 1994. Geomagnetic polarity reversals: a connection with secular variation and core-mantle interaction? *Rev. Geophys.*, **32**, 61–83.

Heider F. and Dunlop D.J., 1987. Two types of chemical remanent magnetizations during oxidation of magnetite. *Phys. Earth Planet. Inter.*, **46**, 24–45.

Heller R., Merril R.T. and McFadden P.L., 2002. The variation of Earth´s magnetic field with time. *Phys. Earth Planet. Inter*., **131**, 237–249.

Hide R., 1967. Motions of the Earth´s core and mantle, and variation of the main geomagnetic field. *Science*, **157**, 55–56.

Johnson C.L., Constable C.G., Tauxe L., Barendregt R., Brown L.L., Coe R.S., Layer P., Mejia V., Opdyke N.D., Singer B.S., Staudigel H. and Stone D.B., 2008. Recent investigations of the 0-5 Ma geomagnetic field recorded by lava flows. *Geochem. Geophys. Geosyst.*, **9**, Q04032.

Kirschvink J.L., 1980. The least-square line and plane and analysis of palaeomagnetic data. *Geophys. J. R. Astron. Soc*., **62**, 699–718.

Kosterov A. and Prévot M., 1998. Possible mechanisms causing failure of Thellier paleointensity experiments: results of rock magnetic study of the Lesotho basalt, Southern Africa. *Geophys. J. Int.*, **134**, 554–572,

Larson R.L. and Olson P., 1991. Mantle plumes control magnetic reversal frequency. *Earth Planet. Sci. Lett.*, **107**, 437–447.

McEllhinny M.W and McFadden P.L., 1997. Paleosecular variation over the past 5 Myr based on a new generalized database. *Geophys. J. Int.*, **131**, 240–252.

McFadden P.L. and Lowes F.J., 1981. The discrimination of mean directions drawn from Fisher distributions. *Geophys. J. R. Astron. Soc.*, **67**, 19–33.

McFadden P.L. and McElhinny M.W., 1990. Classification of the reversal test in paleomagnetism. *Geophys. J. Int*., **103**, 725–729.

McFadden P.L. and Merrill R.T., 1997. Asymmetry in the reversal rate before and after the Cretaceous normal polarity superchron. *Earth Planet. Sci. Lett.*, **149**, 43–47.

McFadden P.L., Merrill R.T. and McElhinny M.W, 1988. Dipole-Quadrupole family modeling of paleosecular variation. *J. Geophys. Res.*, **93**, 11583–11588.

Mena M., Orgeira M.J. and Lagorio S., 2006. Paleomagnetism, rockmagnetism and geochemical aspects of early Cretaceous basalts of the Paraná Magmatic Province, from Misiones, Argentina. *Earth Planets Space*, **58**, 1283–1293.

Muller R.D., Royer J.Y. and Lawver L.A., 1993. Revised plate motions relative to the hotspots from combined Atlantic and Indean Ocean hotspot tracks. *Geology*, **21**, 275–278.

Nagata T., Arai Y. and Momose K., 1963. Secular variation of the geomagnetic total force during the last 5000 years. *J. Geophys. Res*., **68**, 5277–5281.

Néel L., 1955. Some theoretical aspects of rock-magnetism. *Adv. Phys*., **4**, 191–243.

Nishitani T. and Kono M., 1989. Effects of low-temperatures oxidation on the remanence properties of titanomagnetites. *J. Geomagn. Geoelectr.*, **41**, 19–38.

Özdemir Ö., 1987. Inversion of titanomaghemites. *Phys. Earth Planet. Inter.*, **46**, 184–196.

Özdemir Ö. and Dunlop D.J., 1989. Chemico-viscous remanent magnetization in the $Fe_3O_{4-y}Fe_2O_3$ system. *Science*, **243**, 1043–1047.

Piccirillo E.M. and Melfi A.J. (Eds.), 1988. *The Mesozoic Flood Volcanism from the Paraná Basin (Brazil): Petrogenetic and Geophysical Aspects*. Univ. de Sao Paulo, Sao Paulo, Brazil.

Prévot M., Mainkinen R.S., Grommé S. and Lecaille A., 1983. High paleointensity of the geomagnetic field from thermomagnetic studies on rift valley pillow basalts from the middle Atlantic ridge. *J. Geophys. Res.*, **88**, 2316–2326.

Prévot M., Derder M., McWilliams M.M. and Thompson J., 1990. Intensity of the Earth's magnetic field: evidence for a Mesozoic dipole low. *Earth Planet. Sci. Lett.*, **97**, 129–139.

Raposo M.I.B. and Ernesto M., 1995. An Early Cretaceous paleomagnetic pole from Ponta Grossa dikes (Brazil): Implications for the South American Mesozoic apparent polar wander path. *J. Geophys. Res.*, **100(B10)**, 20095–20109.

Raposo M.I.B., Ernesto M. and Renne P.R., 1998. Paleomagnetism and 40Ar/39Ar dating of the early Cretaceous Florianópolis dike swarm (Santa Catarina Island), Southern Brazil. *Phys. Earth Planet. Inter.*, **108**, 275–290.

Readman P. and O'Reilly W., 1972. The synthesis and inversion of nonstoichiometric titanomagnetites. *Phys. Earth Planet. Inter.*, **4**, 121–128.

Renne P., Ernesto M., Pacca I., Coe R.S., Glen J.M., Prévot M. and Perrin M., 1992. The age of Paraná flood volcanism, rifting of Gondwanaland, and Jurassic-cretaceous boundary. *Science*, **258**, 975–979.

Renne P., Glen J.M., Milner S.C. and Duncan A.R., 1996. Age of Etendeka flood volcanism and associated intrusions in southwestern Africa. *Geology*, **24**, 659–662.

Riisager P., Riisager J., Abrahamsen N. and Waagstein R., 2002. Thellier palaeointensity experiments on Faroes flood basalts: technical aspects and geomagnetic implications. *Phys. Earth Planet. Inter.*, **131**, 91–100.

Solano M.C., Goguitchaichvili A., Sánchez Bettucci L., Cejudo Ruiz R., Calvo-Rathert M., Ruiz-Martinez V.C., Soto R. and Alva-Valdivia L.M., 2010. Paleomagnetism of Early Cretaceous Arapey Formation (Northern Uruguay). *Stud. Geophys. Geod.*, **54**, 533–546.

Somoza R. and Zaffarana C., 2008. Mid-Cretaceous polar standstill of South America, motion of the Atlantic hotspots and the birth of the Andean cordillera. *Earth Planet. Sci. Lett.*, **271**, 267–277.

Somoza R., Vizán H. and Taylor G.K., 2005. Rotaciones tectónicas en el Macizo del Deseado durante el desmembramiento de Gondwana. *16º Congreso Geológico Argentino, Actas 1*. Asoc. Geol. Arg., La Plata, Argentina, 403–410.

Tauxe L. and Staudigel H., 2004, Strength of the geomagnetic field in the Cretaceous Normal Superchron: New data from submarine basaltic glass of the Troodos Ophiolite. *Geochem. Geophys. Geosyst.*, **5** ,Q02H06, DOI: 10.1029/2003GC000635.

Tauxe L., Mullender T.A.T. and Pick. T., 1996. Potbellies, wasp-waists, and super-paramagnetism in magnetic hysteresis. *J. Geophys. Res*., **101**, 571–583.

Tarduno J.A., Cottrell R.D. and Smirnov A.V., 2001. High geomagnetic intensity during the Mid-Cretaceous from Thellier analyses of single plagioclase crystals. *Science*, **291**, 1779–1783.

Tarduno J.A., Cottrell R.D. and Smirnov A.V., 2002. The Cretaceous superchron geodynamo: observations near the tangent cylinder. *Proc. Natl. Acad. Sci. U. S. A.*, **99**, 14020–14025.

Thellier E. and Thellier O., 1944. Recherches géomagnetiques sur les coulees volcaniques d'Auvergne: *Ann. Géophys.*, **1**, 37–52.

Thellier E. and Thellier O., 1959. Sur l'intensité du champ magnétique terrestre dans le passé historique et géologique. *Ann. Géophys*., **15**, 285–376.

Turner S., Regelous M., Kelley S., Hawkesworth C.J. and Mantovani M.M.S., 1994. Magmatism and continental break-up in the South Atlantic: high precision 40Ar-39Ar geochronology. *Earth Planet. Sci. Lett*., **121**, 333–348.

Valet J.-P. and Herrero-Bervera E., 2000. Paleointensity experiments using alternating field demagnetization. *Earth Planet. Sci. Lett.*, **177**, 43–53.

Xu T.C., Tarling D.H., Eustance N.B. and Hijab B.R., 1986. Short term viscous effects on measurements of remanence. *Geophys. J. R. Astron. Soc*., **87**, 305–309.

Zijderveld J.D., 1967. A.C. Demagnetization in rocks: analysis of results. In: Collinson D.W., Creer K.M. and Runcorn S.K. (Eds.), *Methods in Paleomagnetism*. Elsevier, New York, 254–286.